JCI The Journal of Clinical Investigation

TRIP13 modulates protein deubiquitination and accelerates tumor development and progression of B-cell malignancies

Can Li, … , Ivana Frech, Fenghuang Zhan

J Clin Invest. 2021. https://doi.org/10.1172/JCI146893.

Research In-Press Preview **Hematology**

Graphical abstract

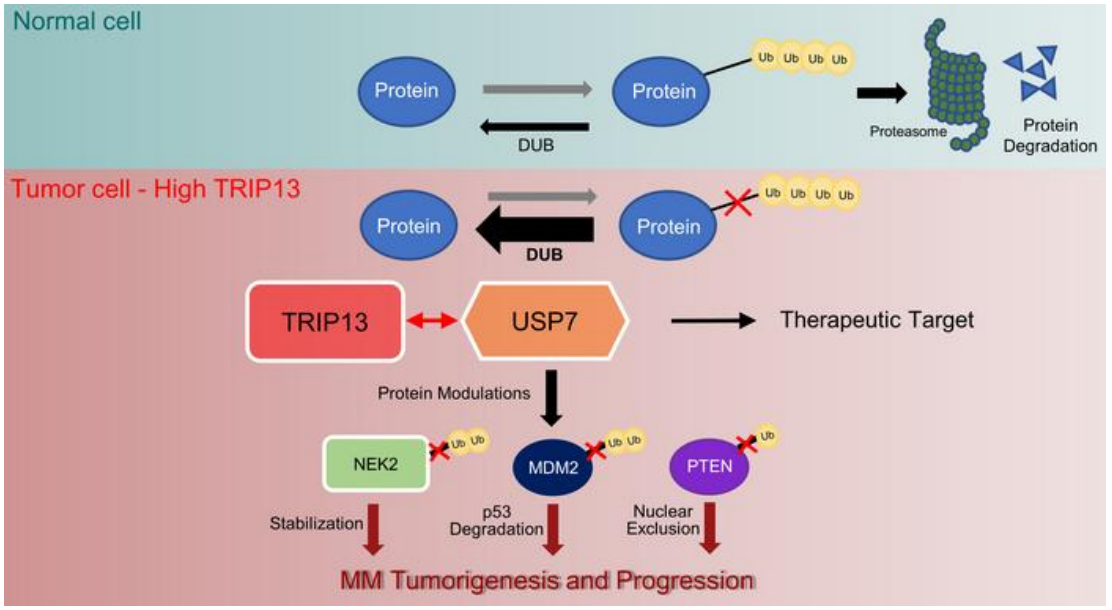

TRIP13 modulates protein deubiquitination and accelerates tumor development and progression of B-cell malignancies

Can Li[1,2], Jiliang Xia[3], Reinaldo Franqui-Machin[3], Fangping Chen[2], Yanjuan He[2], Timothy Cody Ashby[1], Feixiang Teng[1], Hongwei Xu[1], Dingxiao Liu[3], Dongzheng Gai[1,2], Sarah K Johnson[1], Frits van Rhee[1], Siegfried Janz[4], John D Shaughnessy Jr[1], Guido Tricot[1], Ivana Frech[3], Fenghuang Zhan[1*]

[1]Myeloma Center, Winthrop P. Rockefeller Cancer Institute, Department of Internal Medicine, University of Arkansas for Medical Sciences, Little Rock, Arkansas, USA.

[2]Department of Hematology, Xiangya Hospital, Central South University, Changsha, Hunan, China.

[3]Department of Internal Medicine, University of Iowa, Iowa City, Iowa, USA.

[4]Division of Hematology and Oncology, Department of Medicine, Medical College of Wisconsin, Milwaukee, Wisconsin, USA.

[*]Correspondence to: Fenghuang Zhan FZhan@uams.edu

Mailing address: 4301 W. Markham St. Slot# 508, Little Rock, AR, USA 72205

Tel: 501-526-6000 ext. 25228

The authors have declared that no conflict of interest exists.

Abstract

Multiple myeloma (MM), a terminally differentiated B-cell malignancy, remains difficult to cure. Understanding the molecular mechanisms underlying the progression of MM may identify therapeutic targets and lead to a fundamental shift in treatment of the disease. Deubiquitination like ubiquitination is a highly regulated process, implicated in almost every cellular process. Multiple deubiquitinating enzymes (DUBs) have been identified but their regulation is poorly defined. Here, we determined that TRIP13 increases cellular deubiquitination. Overexpression of TRIP13 in mice and cultured cells resulted in excess cellular deubiquitination by enhancing the association of the DUB USP7 with its substrates. We show that TRIP13 is an oncogenic protein because it accelerates B-cell tumor development in transgenic mice. TRIP13-induced resistance to proteasome inhibition can be overcome by a USP7 inhibitor in vitro and in vivo. These findings point to a critical role for TRIP13 expression in B-cell lymphoma and MM by governing deubiquitination of critical oncogenic (NEK2) and tumor suppressor (PTEN, P53) proteins. High TRIP13 identifies a high-risk patient group amendable to adjuvant anti-USP7 therapy.

Introduction

Multiple myeloma (MM), a malignancy of terminally differentiated antibody-secreting plasma cells, can be separated into high- and low-risk based on the differential expression of 70 genes on gene expression profiling (GEP) (1). High risk GEP, present in approximately 20% of newly diagnosed disease, is characterized by the increased expression of 52 genes, the majority of which map to chromosome 1q, combined with reduced expression of 18 genes, the majority of which map to chromosome 1p. While the combination of autologous stem cell transplantation (ASCT) with novel agents, such as proteasome inhibitors, immunomodulatory agents and monoclonal antibodies (2, 3) has significantly improved progression-free and overall survival (OS) in low-risk disease, the dismal outcome of high-risk disease remains a significant clinical problem (4). Also, the acquisition of a high-risk signature at disease relapse is linked to shorter post-relapse survival, strongly suggesting that high-risk cells, representing only a small fraction of tumor bulk at diagnosis in low-risk disease, but surviving chemotherapeutic interventions (1). Consistent with this concept, copy number of chromosome 1q and the percentage of cells with 1q gains both increase at relapse in a significant fraction of cases of MM (5). These data suggest that chromosome 1q copy number gains are a likely driver of aggressive tumor behavior. The GEP70 signature not only represents a highly robust collection of risk biomarkers, its composition also reveals key biological features of disease progression, and potential targets for therapeutic intervention.

The gene Thyroid Hormone Receptor Interacting Protein 13 (*TRIP13*), represents one of the genes within the 70-gene signature overexpressed in high risk MM (1) and is also one of 10 genes constituting a chromosome instability (CIN) signature in MM (6). In

addition to MM (7, 8), high *TRIP13* expression is associated with aggressive disease in chronic lymphocytic leukemia (9), prostate cancer (10, 11), breast cancer (12, 13), colorectal cancer (14), hepatocellular carcinoma (15), lung cancer (16, 17) and neck and head cancer (18).

TRIP13 is a member of the AAA$^+$ (**A**TPases **a**ssociated with diverse cellular **a**ctivities)-ATPase family of proteins that alter the conformation of client macromolecules and thereby affect cellular signaling. This enzyme is involved in various cellular biological processes and is classically considered a regulator of chromosomal events including chromosome synapsis, checkpoint signaling and DNA break formation and recombination (19). Premature exit from the spindle assembly checkpoint blocks DNA repair and leads to mis-segregation of chromosomes, causing both structural and numerical aneuploidy events. Recent studies have shown that high levels of TRIP13 promote both the non-homologous end joining (NHEJ) and the homology-directed repair (HDR) of double-strand breaks (DSBs) (18, 20), potentially leading to CIN, cancer cell survival, metastasis, and enhanced drug resistance.

The ubiquitin proteasome system (UPS) enables a dynamic homeostasis of proteins through a highly regulated process of protein ubiquitination and proteasomal degradation. The UPS is deregulated in MM and represents a potential target of intervention for MM therapy. By comparing gene expression profiles of MM cells prior to and after administration of a test dose of the proteasome inhibitor, bortezomib (BTZ), we were able to show that upregulation of the proteasome within 48 hours of drug administration is associated with poor outcome in MM patients treated with Immunomodulatory drugs (IMiDs), proteasome inhibitors and ASCT (21). The

centrosomal kinase, Never in Mitosis (NIMA) Related Kinase 2A (*NEK2*), mapping to chromosome 1q, is another copy number sensitive gene in MM and expressed at elevated levels in high-risk MM and other cancers (6, 22, 23). NEK2 increases proteasome activity in MM cells (24), binds to and is stabilized by the deubiquitinase ubiquitin-specific protase-7 (USP7, also known as HAUSP) leading to the activation of the canonical NF-kappa B signaling pathway resulting in increased drug resistance and bone destruction (25, 26). TRIP13 expression causes spindle assembly checkpoint errors through enhanced ubiquitin-mediated, proteasomal degradation of MAD2 (7).

Here, we provide further evidence that TRIP13 enhances cellular protein deubiquitination by binding the deubiquitinase USP7. Moreover, we show that TRIP13 plays a critical role in stabilizing NEK2 via a TRIP13/USP7-dependent mechanism. Using a small-molecule inhibitor of USP7, we have targeted the TRIP13/USP7/NEK2 complex and shown that this intervention abrogates B-cell tumorigenesis and overcomes drug resistance.

Results

Generation of Trip13 tissue-specific transgenic murine model.

To determine if Trip13 can drive lymphoid-derived tumorigenesis, we inserted the complete coding region of mouse *Trip13* into the p1026x-HA3P vector (27). The p1026x vector includes a 3.2 kb fragment of the proximal promoter of the mouse Lck gene, a 0.92 kb fragment of the Eμ enhancer and a 2.1 kb mutated (non-translatable) version of the human growth hormone gene (HGx) driving expression in T- and B-cells (**Figure 1A**). Three lines were selected and backcrossed to a C57BL/6 background for at least ten generations (**Figure 1B**). Western blotting was employed to confirm the tissue-specific expression of Trip13 protein in transgenic (*Trip13*^{TG}) mice relative to wild-type (*Trip13*^{WT}) littermate mice. **Figure 1C** shows that Trip13 protein was endogenously expressed in mouse spleen, thymus and bone marrow, and was significantly increased in *Trip13*^{TG} mice. As expected, testis as a positive control expressed high Trip13 protein in both *Trip13*^{TG} and *Trip13*^{WT} mice while lung, liver and kidney had no detectable expression. To further determine the cell specificity of *Trip13* expression, we enriched B cells from spleen and T cells from thymus of *Trip13*^{TG} mice using B and T lymphoid lineage specific antibody (B220 and CD3)-conjugated magnetic beads. Western blots of protein isolated from enriched cells showed that Trip13 protein was dramatically increased in *Trip13*^{TG} mice compared to *Trip13*^{WT} mice in B220^{+} B cells and CD3^{+} T cells but not in CD11b^{+} granulocytes (**Figure 1D**). There was no significant difference in the survival of *Trip13*^{TG} mice relative to *Trip13*^{WT} mice, nor in lymphoid tissue sizes (Supplemental Figure 1). To further investigate whether lymphoid lineage subsets changed with *Trip13* transgene, we performed flow cytometry on mice spleen, LN,

thymus and BM, and found that percentages of both B- and T-lineage subsets were similar in *Trip13*^{TG} mice compared to *Trip13*^{WT} littermate controls (data not shown).These data strongly suggest that Trip13 overexpression by itself does not initiate tumorigenesis, as is the case with most oncogenes.

Eμ-*Myc*/*Trip13*^{TG} mice develop an aggressive B-cell malignancy.

The *MYC* oncogene is widely dysregulated in a variety of human cancers, including MM, lymphomas and solid tumors (28-30) and the Eμ-*Myc* mouse is a well-established preclinical model for B-cell malignancies including diffuse high-grade lymphomas, diffuse large B-cell lymphomas (DLBCLs), and plasmacytomas (31, 32). To determine whether *Trip13* does cooperate with *Myc* in tumorigenesis, we crossed the *Trip13*^{TG} with the Eμ-*Myc* mice. Mouse survival was compared between Eμ-*Myc* mice and Eμ-*Myc*/*Trip13*^{TG} mice. The Eμ-*Myc*/*Trip13*^{TG} mice developed tumors at a younger age than the Eμ-*Myc* mice, resulting in a significantly shorter survival (median survival Eμ-*Myc*/*Trip13*^{TG} mice 106 days versus Eμ-*Myc*/*Trip13*^{WT} mice 141 days, $P = 0.0002$, **Figure 1E**). With lymphoma progression, mice developed pronounced cervical, inguinal, axillary and intestinal lymphadenopathy, splenomegaly and an enlarged thymus (Supplemental Figure 2A and 2B), respiratory distress, hunched posture, limited mobility and paralysis. Flow cytometry (Supplemental Figure 2C and 2D) further confirmed that the spontaneous tumors were lymphomas of B-cell origin. Thus, *Trip13* cooperates with *Myc* to accelerate the development of B-cell malignancies.

Elevated *TRIP13* expression is linked to poor prognosis.

We examined whether elevated expression of *TRIP13* is associated with inferior clinical outcome in DLBCLs and MM. Kaplan-Meier analysis based on *TRIP13* expression levels in DLBCL demonstrated a significantly inferior OS associated with high *TRIP13* (Using best cut off) (**Figure 1F**, $P = 0.0003$). Interestingly, this association was specific to activated B-cell DLBCLs (ABC DLBCLs) (Supplemental Figure 2E, $P = 0.01573$), but was not observed in germinal center or unclassified B-cell DLBCLs. ABC DLBCLs have been associated with a significantly worse OS compared to GCB DLBCLs (33, 34). Our data indicate that TRIP13 expression is a significant prognostic factor in ABC DLBCL. In an independent MM dataset- the CoMMpass dataset, Kaplan-Meier analysis of MM patients also validated a significantly inferior OS associated with high *TRIP13* (Quartile 4) (**Figure 1G**, $P < 0.0001$), confirming our earlier findings in MM patients treated with tandem transplants (7).

TRIP13 enhances cellular protein deubiquitination.

To further characterize the role of Trip13 in Eμ-*Myc*-induced B-cell malignancies, we collected pre-malignant B cells ($B220^+$) from both Eμ-*Myc*/*Trip13*^{TG} and Eμ-*Myc*/*Trip13*^{WT} mice at 6 weeks of age and performed RNA-sequencing analyses. As shown in **Figure 2A**, more than 1,900 genes were differentially expressed in B cells from these two strains ($P < 0.001$). We then analyzed signaling pathways using Gene Ontology (GO) and Kyoto Encyclopedia of Genes and Genomes (KEGG). The GO analysis revealed that proteasome-mediated and ubiquitination-dependent GO genes

were significantly enriched for biological processes (BP), cellular components (CC) and molecular functions (MF) in Eμ-*Myc*/*Trip13*^{TG} mice (**Figure 2B,** $P < 10^{-7}$). In the MF group, 4 of the top 10 upregulated GO terms were associated with ubiquitin-related pathways. KEGG analysis confirmed that the ubiquitin-mediated proteolysis pathway was significantly enriched (**Figure 2C**). To determine the relationship between high TRIP13 and sensitivity to chemotherapeutic drugs in MM, the MM cell lines ARP1 and H929, with or without TRIP13 overexpression, were treated with the alkylating agent melphalan, the DNA-damaging topoisomerase inhibitor etoposide, or the proteasome inhibitor BTZ (Supplemental Figure 3). TRIP13 overexpression only prevented BTZ-induced cell death but did not alter sensitivity to melphalan or etoposide. Our clinical experience, however, indicates that a combination of BTZ, IMiDs, and ASCTs does not markedly improve patient outcome in MM with a high-risk GEP70 score or high *TRIP13.* These findings suggest that TRIP13 may play a significant role in regulating drug response through its ability to modulate the ubiquitin-proteasome system within tumor cells.

To address this possibility further, we examined the effect of TRIP13 expression on cellular ubiquitination. In TRIP13-overexpressed ARP1 and H929 MM cell lines, the total cellular ubiquitinated protein levels were significantly decreased compared to those cells transfected with empty vector (EV) (**Figure 2D**, lanes 1 versus 2; Supplemental Figure 4). Inhibition of protein degradation with the proteasome inhibitor, BTZ, highlights the decreased cellular ubiquitination seen in TRIP13 OE cells compared to EV cells (**Figure 2D**, lane 3 versus 4). We further examined the relationship between TRIP13 and cellular ubiquitin levels by using ARP1 cells stably transfected with a doxycycline (DOX)-

inducible vector expressing TRIP13 shRNA. Knockdown of TRIP13 resulted in elevated ubiquitinated proteins and this was even more pronounced upon treatment with BTZ (**Figure 2E**). To confirm this observation in vivo, we employed the newly developed *Trip13*^{TG} mice. Immunoblotting for ubiquitinated proteins in *Trip13*^{TG} mice showed a decreased signal in both thymus (**Figure 2F**, lane 1 and 3) and spleen tissue (**Figure 2F**, lane 2 and 4) relative to *Trip13*^{WT} littermate controls.

TRIP13 enhances cellular deubiquitination by binding USP7.

To evaluate how TRIP13 enhances cellular deubiquitination, we took advantage of the fact that overexpression of TRIP13 induces a BTZ-resistant phenotype in MM and other cancer cells. Using ARP1 and H929 MM cell lines, we tested a series of widely used ubiquitination and de-ubiquitination inhibitors, such as PYR-41 (E1 inhibitor), PR-619 (non-selective USPs inhibitor), Spautin-1 (USP10 inhibitor) or P5091 (USP7 inhibitor). Cell viability analysis showed that only the USP7 inhibitor P5091 reduced TRIP13-mediated drug resistance (Supplemental Figure 5).

We analyzed the ubiquitin levels in ARP1 EV and ARP1 TRIP13 OE cells treated with the USP7 inhibitor P5091 overnight, with or without BTZ. TRIP13 OE cells showed lower ubiquitination when compared to EV cells (**Figure 3A,** lane 1 versus lane 5 and lane 2 versus lane 6). However, this decrease was reversed by the P5091 treatment (**Figure 3A**, lane 3 versus lane 7 and lane 4 versus lane 8). Since there is a high correlation of TRIP13, NEK2 and USP7 (25), USP7 might interact with TRIP13 to mediate cellular deubiquitination.

To evaluate whether TRIP13 acts as a DUB or regulates USP7 activity, we performed an in vitro deubiquitination assay using two different ubiquitin substrates: K63 and K48. Western blot analysis showed that purified TRIP13 did not change the ubiquitination of K63 (**Figure 3B,** lane 5 versus lane 1) or K48 (**Figure 3C,** lane 5 versus lane 1), suggesting that TRIP13 does not function as a DUB. Commercially available recombinant USP7 proteins were able to degrade ubiquitin (**Figure 3B and 3C,** lane 3 versus lane 1) and this degradation was inhibited when the deubiquitinase inhibitor, N-Ethylmaleimide (NEM) was added to the in vitro deubiquitination assays (**Figure 3B and 3C,** lane 4 versus lane 3). As shown in **Figure 3B and 3C** (lane 3 versus lane 1), the DUB USP7 released the ubiquitin monomeric form (indicated by black arrows) while poly-ubiquitin chains were degraded in vitro. We observed that the USP7-mediated ubiquitin degradation was further enhanced by the addition of TRIP13 as evidenced by a stronger signal of ubiquitin monomers released (**Figure 3B and 3C**, lane 5 versus lane 1). These data indicate that TRIP13 enhances USP7-mediated ubiquitin degradation.

To determine whether TRIP13 binds to USP7, a co-immunoprecipitation of endogenous TRIP13 in ARP1 cells was performed using TRIP13 antibodies. USP7 was found to bind to endogenous TRIP13 (**Figure 3D**, TRIP13 IP). This result was also confirmed by TRIP13-FLAG overexpression and immunoprecipitation in H1299 cells using anti-FLAG antibodies (Supplemental Figure 6). To further confirm that Trip13 binds to Usp7 in vivo, a Trip13 immunoprecipitation was performed on thymus protein lysates isolated from *Trip13*^{TG} mice and compared to *Trip13*^{WT} littermate controls (**Figure 3E**). Western blots detected that Usp7 was bound to Trip13 in *Trip13*^{TG} mice.

This association was not detected in *Trip13*^{WT} littermate controls, most likely because endogenous Trip13 levels were too low to detect USP7 binding by western blotting.

TRIP13 plays a critical role in stabilizing the USP7 target, NEK2.

NEK2 protein binds to USP7, and USP7 stabilizes NEK2, resulting in increased drug resistance to proteasome inhibition (25). To explore whether TRIP13 and NEK2 interact with each other, we performed western blot analysis for NEK2 in cell lysates from ARP1 EV and TRIP13 OE MM cells. Our results showed that TRIP13 overexpression led to an increase in total NEK2 expression (**Figure 4A**). Similar results were observed in 3T3 cells (Supplemental Figure 7A) and in cell lysates from *Trip13*^{TG} mice (**Figure 4B**). Transfection of cells with a TRIP13 shRNA resulted in decreased NEK2 protein (Supplemental Figure 7B and 7C). To address whether the observed increase in NEK2 is mediated by USP7 deubiquitination, ubiquitinated NEK2 levels were assessed. Western blot analysis revealed that the NEK2 ubiquitination signal was reduced when TRIP13 was overexpressed, while USP7 protein was increased (**Figure 4C,** upper panel). As an additional control, we treated those cells with BTZ prior to cell lysis and immunoprecipitation. Similar levels of NEK2 were pulled down in both EV and TRIP13 OE cells treated with BTZ. However, there was less ubiquitinated NEK2 in the presence of elevated TRIP13 (**Figure 4C,** lower panel). Additionally, when NEK2 was immunoprecipitated, USP7 and TRIP13 protein were found to be bound to NEK2. Similar results were observed in H1299 cells when TRIP13 was immunoprecipitated using HA antibodies (Supplemental Figure 7D). These results strongly suggest that TRIP13 physically interacts with USP7 and NEK2 to promote NEK2 deubiquitination.

To determine if TRIP13 binding to USP7 and NEK2 was critical for NEK2 deubiquitination, we analyzed the binding between USP7 and NEK2 in the absence of TRIP13. Using NEK2 antibody to pull down binding proteins, USP7 levels were significantly lower in ARP1 cells lacking TRIP13 (**Figure 4D**, TRIP13 shRNA) compared to controls. These data indicate that TRIP13 mediates the interaction of USP7 with NEK2.

As in Figure 1G, we have previously shown that high *TRIP13* is linked to a shorter OS of MM patients. Using the CoMMpass dataset, we further found that MM patients with high *TRIP13* and high *NEK2* (both Quartile 4) had an inferior OS (**Figure 4E,** $P < 0.0001$) compared to disease with low *TRIP13* / low *NEK2,* low *TRIP13* / high *NEK2* ($P = 0.0228$) or high *TRIP13* / low *NEK2* ($P = 0.0093$). Kaplan-Meier analysis of a UAMS microarray dataset also showed that MM with high *TRIP13* / high *NEK2* (both Quartile 4) is associated with an inferior outcome compared to the disease lacking elevated expression of both genes (Supplemental Figure 7E, $P < 0.0001$). A strong correlation between the expression of *TRIP13* and *NEK2* was found in both the CoMMpass (**Figure 4F,** $r = 0.8128$, $P < 0.0001$) and the UAMS datasets (Supplemental Figure 7F, $r = 0.7091$, $P < 0.0001$). These data suggest that elevated expression of both *TRIP13* and *NEK2* is linked to a more aggressive clinical phenotype in MM. Gene Set Enrichment Analysis (GSEA) from CoMMpass shows that ubiquitin-mediated proteolysis pathways are significantly enriched in MM patients with high *TRIP13* and both high *TRIP13* / high NEK2, but not in those with high *NEK2,* but low *TRIP13* (Supplemental Figure 8).

TRIP13 dysregulates other USP7 targets.

USP7 stabilizes multiple oncogenes (35) resulting in PTEN nuclear exclusion (36) and p53 degradation (37). To test whether TRIP13 was involved in USP7-mediated oncogene stabilization, we performed GSEA on the RNA-sequencing data of Eμ-*Myc*/*Trip13*^{TG} and Eμ-*Myc*/*Trip13*^{WT} mice B cells (**Figure 5A**). Ten significant pathways distinguished B cells of the Eμ-*Myc*/*Trip13*^{TG} mice from the Eμ-*Myc*/*Trip13*^{WT} mice. PTEN and p53 signaling were significantly suppressed by *Trip13* (**Figure 5B**). We then analyzed PTEN localization in MM cells overexpressing TRIP13. Immunoblotting on nuclear and cytoplasmic fractions was performed in EV and TRIP13 OE ARP1 cells. The data confirmed that nuclear PTEN was significantly reduced in TRIP13 OE ARP1 cells (**Figure 5C**) when compared to EV ARP1 cells. We then analyzed nuclear levels of PTEN when TRIP13 was knocked down (**Figure 5D**, TRIP13 shRNA) and found that in the absence of TRIP13, there was an enrichment of nuclear PTEN. Consistent with these in vitro data, nuclear Pten was undetectable in *Trip13*^{TG} mice, but it was detectable in *Trip13*^{WT} littermate control (**Figure 5E**). We further investigated whether USP7 inhibition could increase nuclear PTEN in TRIP13 OE MM cells. Indeed, similar levels of nuclear PTEN were observed in P5091 treated TRIP13 EV and OE ARP1 cells (**Figure 5F**). The p53 protein was barely detectable in *Trip13*^{TG} mice thymus relative to *Trip13*^{WT} littermate controls (**Figure 5G**). These results indicate that TRIP13 regulates levels of Pten and Tp53.

The AAA^{+}-ATPase of TRIP13 is required for USP7 deubiquitinase function.

To evaluate how TRIP13 regulates USP7 activity, we first analyzed the level of USP7 phosphorylation. No difference was detected in USP7 phosphorylation between EV and

TRIP13 OE ARP1 cells (Supplemental Figure 9). We next tested whether stabilization might be an ATP-dependent process driven by TRIP13 as reported for the TRIP13comet-C-MAD2-CDC20 complex (38). Treatment of TRIP13 OE ARP1 cells with oligomycin, an inhibitor of ATPase synthase (39), followed by TRIP13 immunoprecipitation revealed that TRIP13 was not bound to USP7 (**Figure 6A**). We also generated two C-terminal deletion TRIP13 constructs lacking the ATPase domain, one lacking the first 100 amino acids (Δ1) and a second missing the first 200 amino acids (Δ2). HEK293T cells were transduced with TRIP13 WT or truncated constructs (Δ1 and Δ2 in combination with WT FLAG-USP7). Immunoprecipitation using HA antibody followed by western blot analysis showed that TRIP13 WT was binding USP7 while TRIP13 Δ1 and Δ2 failed to do so (**Figure 6B**). We employed the TRIP13 ATP hydrolysis-defective mutant TRIP13-E253Q (40) in an in vitro deubiquitination time course. As shown in **Figure 6C**, USP7 alone could not degrade ubiquitin within 15-minutes (**Figure 6C,** red arrow). In the presence of TRIP13-WT, ubiquitin degradation was detected at 15 minutes (**Figure 6C**, blue arrow) whereas TRIP13-E253Q did not enhance USP7-mediated ubiquitin degradation. Remarkably, not only did we observe that TRIP13-E253Q did not enhance USP7 DUB activity, but no ubiquitin degradation was detected at all within the 30-minute timeframe of the assay (**Figure 6C**, green arrow). These data indicate that 1) TRIP13 enhances and accelerates USP7-mediated ubiquitin degradation, 2) TRIP13 ATP hydrolysis is required for TRIP13/USP7 DUB activity, and 3) TRIP13 ATPase is required for TRIP13-USP7 binding as well as for the subsequent DUB activity of USP7.

The USP7 inhibitor reduces TRIP13-induced BTZ drug resistance in MM.

As shown in **Figure 7A and 7B**, TRIP13 OE ARP1 and H929 MM cells were markedly resistant to BTZ, while TRIP13 EV MM cell lines were sensitive. However, by adding P5091 to BTZ, TRIP13 OE MM cells were rendered BTZ sensitivity, demonstrating that USP7 inhibition reduces TRIP13-induced BTZ drug resistance in MM cells. We tested the effects of P5091 on TRIP13 OE and EV ARP1 MM cells grown in the NSG subcutaneous xenograft mouse model. Mice injected with EV cells on the left flank and TRIP13 OE cells on the right flank were grouped and treated with vehicle control, P5091 (10mg/kg, *i.v.*, twice a week from day 3), BTZ (1mg/kg, *i.p.*, twice a week from day 7) or a combination of P5091 and BTZ. As shown in the pictures of dissected tumors (**Figure 7C**), TRIP13 significantly enhanced MM tumor growth and BTZ had little effect in reducing the TRIP13 OE MM tumor burden. However, P5091 alone and in combination with BTZ significantly reduced MM tumor size (**Figure 7D and 7E**). We also confirmed that TRIP13 mRNA and protein expression are strongly correlated in primary MM samples (**Figure 7F**). To further validate the clinical relevance of USP7 inhibition reducing TRIP13-induced BTZ drug resistance, we performed ex vivo treatment on 6 low *TRIP13* and 6 high *TRIP13* primary CD138-positive MM samples as determined by TRIP13 gene expression signal. *TRIP13* gene expression signals of these individual primary CD138-positive MM samples were analyzed. In agreement with in vitro MM cell line results, primary MM cells with high *TRIP13* exhibited drug resistance to BTZ; however, combination treatment with P5091 and BTZ significantly reduced MM cell viability, while primary MM cells with low *TRIP13* were sensitive to both BTZ and combination treatment (**Figure 7G**). The additive/synergistic effect of BTZ and P5091

suggests that combined USP7 and proteasome inhibition overcomes TRIP13 and NEK2-induced MM drug resistance and tumor growth.

Usp7 inhibition abrogates B-cell lymphomas in vivo.

To investigate the effects of Usp7 inhibition on B-cell lymphomas in vivo, we generated B-cell tumors in recipient wild-type syngeneic C57BL/6 mice by transplantation of spontaneously arising Eμ-*Myc*/*Trip13*^{WT} and Eμ-*Myc*/*Trip13*^{TG} lymphoma cells. Mice transplanted with Eμ-*Myc*/*Trip13*^{TG} cells exhibited a shorter survival compared to mice transplanted with Eμ-*Myc*/*Trip13*^{WT} cells (**Figure 8A**, $P = 0.0085$). This result indicates that overexpression of Trip13 in Eμ-*Myc* produces a more aggressive B-cell malignancy, consistent with results of double transgenic Eμ-*Myc*/*Trip13*^{TG} mice in **Figure 1E** and the MM xenograft model in **Figure 7C**. Compared with vehicle controls, treatment with P5091 significantly improved the survival of mice transplanted with both Eμ-*Myc*/*Trip13*^{WT} lymphoma cells (**Figure 8B**, blue dotted line versus black dotted line, median survival 33 days versus 27 days) and the more aggressive Eμ-*Myc*/*Trip13*^{TG} lymphoma cells (**Figure 8C**, blue solid line versus black solid line, median survival 32 days versus 21 days). Single agent treatment with doxorubicin, a cytotoxic agent used to treat lymphoma, was highly efficacious in recipient mice bearing Eμ-*Myc*/*Trip13*^{WT} lymphoma (**Figure 8B**, red dotted line). The combination of doxorubicin and P5091 further extended mouse survival (Combination treatment median survival 67 days versus doxorubicin only 54 days). The median survival of mice bearing Eμ-*Myc*/*Trip13*^{TG} lymphoma treated with single agent doxorubicin was only 39 days compared to 21 days in vehicle control treated animals, indicating decreased efficacy of doxorubicin in Trip13

overexpressing B-cell lymphomas. However, mice bearing Eμ-*Myc*/*Trip13*^{TG} lymphomas survived a median of 49 days when treated with the combination of doxorubicin and P5091.

To further confirm that Usp7 inhibition decreased lymphoma tumor burden, we took advantage of C57BL/6 congenic strain expressing the CD45.1 allele to distinguish host cells from donor tumor cells expressing the CD45.2 allele. Both vehicle control and P5091 treated mice were sacrificed once vehicle control mice achieved the preset endpoint; flow cytometry was performed to evaluate tumor burden. Eμ-*Myc*/*Trip13*^{TG} donor lymphoma cell population ($CD45.2^{+}CD45.1^{-}B220^{+}IgM^{-}$) significantly decreased after P5091 treatment in both lymph nodes (**Figure 8D**) and spleen (**Figure 8E**), demonstrating that P5091 inhibits Eμ-*Myc*/*Trip13*^{TG} driven lymphoma growth.

Discussion

The dramatic difference in survival of MM patients with high and low risk disease, reflected in tumor cell GEP, can be traced to specific chromosomal lesions, namely gains of chromosome 1q and losses of chromosome 1p. Through sequential GEPs, we have demonstrated that TRIP13 expression is correlated with disease progression and drug resistance in MM (6). The important role of TRIP13 in cancer extends beyond MM, with elevated TRIP13 expression correlated to poor prognosis in multiple malignancies (9-16, 18). These observations highlight TRIP13 as a potential therapeutic target.

Here, we present evidence of a novel role for TRIP13 in the modulation of ubiquitin homeostasis of B-cell malignancies. We demonstrate the clinical importance of high TRIP13 expression associated with inferior patient outcomes. Using a transgenic murine model, RNA sequencing and systemic in vitro and in vivo biochemical approaches, we have shown that TRIP13 enhances cellular deubiquitination by binding the deubiquitinase USP7, resulting in a decrease in cellular ubiquitination levels as observed upon stable TRIP13 overexpression in MM cells and in transgenic mice. Applying in vitro kinase assays of poly-ubiquitin chains K48 and K63, we demonstrated that the decreased ubiquitination was not the result of endogenous catalytic activity of TRIP13 but occurs through TRIP13 interaction with the deubiquitinase USP7. The type of ubiquitination modification determines the cellular fate and function of the protein. Mono-Ub is involved in endocytosis, protein transport, histone regulation and DNA repair while multi-Ub is mostly involved in endocytosis and poly-Ub is involved in various cellular processes (41). Poly-ubiquitin chains formed on lysine 48 (K48) of ubiquitin have a well-established role in targeted protein degradation by the 26S

proteasome (42), whereas poly-ubiquitin chains formed on lysine 63 (K63) are involved in DNA repair and endocytosis. However, a recent study showed that K63 ubiquitylation also triggers proteasomal degradation (43). Our in vitro ubiquitinase studies on both K48 and K63 poly-Ub chains highlighted the potential cellular function of TRIP13 / USP7 complex in the modulation of substrate proteasomal degradation.

Our findings of TRIP13 involvement in deubiquitination pathways are novel and in agreement with findings of other investigators demonstrating that AAA$^+$-ATPases are able to bind DUBs and promote their activity. For example, p97 has been shown to recruit and promote deubiquitination activity of several DUBs, such as vcip135, Otu1, YOD1 and others (44, 45). We hypothesized that TRIP13 AAA$^+$-ATPase activity would provide the chemical energy for the ATP-dependent ubiquitin-protease activity of USP7. Indeed, the AAA$^+$-ATPase defective TRIP13 E253Q mutant abrogated the in vitro deubiquitinase activity of USP7. USP7 maintained deubiquitination even in the absence of TRIP13, indicating that TRIP13 does not provide ATP for USP7 deubiquitination. The presence of TRIP13, however, leads to a more rapid and more thorough deubiquitination by USP7. These results indicate that TRIP13 binding promotes USP7 deubiquitination activity and that a mutation of TRIP13 at Glutamate-253 disrupts this binding. While the crystallization of TRIP13 with USP7 has not been performed, we would predict that TRIP13 binding to USP7 occurs in the UBL 1-3 region and that a mutation at E253Q would disrupt this interaction sufficiently to interfere with the stabilization of the USP7 switching loop. Early evidence including point mutation and C-terminal deletion in TRIP13 suggests that this binding of USP7 is dependent upon the carboxy terminus of TRIP13.

Ubiquitination can mediate protein function through changes in localization, stability, and interactions. PTEN (36, 46) and p53 (37, 47-49), each exert a critical function in regulating genomic stability, and are USP7 targets. In this study, we found that TRIP13 dysregulates these well-known USP7 targets resulting in tumor progression. Specifically, we found evidence that TRIP13 causes the nuclear exclusion of the tumor suppressor PTEN and leads to decreased stability of p53. Application of the USP7 small molecule inhibitor P5091, demonstrated that these activities of TRIP13 occur through the deubiquitinase USP7. Data presented in this work indicate that increased TRIP13 activity suppresses the TP53 pathway and as such indicate that this might be an alternative pathway to disable TP53 activity in MM and other malignancies, not requiring inactivation of TP53 by deletion or mutations. Future work will be aimed at studying the interplay between TRIP13 and TP53.

Elevated expression of the NEK2 gene is highly correlated with CIN, drug resistance, and poor prognosis in MM (6, 26). We recently discovered that NEK2 protein binds to the DUB, USP7. USP7 stabilizes NEK2 by preventing proteasomal degradation of NEK2 in MM cells, resulting in increased drug resistance, which is a prominent feature of the high-risk phenotype (25). We also showed that TRIP13 plays a critical role in stabilizing NEK2 through its interaction with USP7. GSEA from CoMMpass indicates that in high-risk MM, TRIP13 and not NEK2, primarily exerts a ubiquitin-mediated proteolysis function; this ubiquitination process appears to have an additive effect in high-risk MM patients. Importantly, using a small-molecule inhibitor of USP7 in vivo in both the MM xenograft and B-cell lymphoma mouse models, we have shown that abrogation of USP7 function leads to reduced tumor growth and decreased drug

resistance. This study reveals a novel function of TRIP13 in cancer biology and identifies the TRIP13/USP7/NEK2 complex as a promising target of therapeutic intervention for high-risk MM.

Our findings provide three focal points for therapeutic intervention in high-risk MM: 1) direct targeting of TRIP13, which has already shown good efficacy (50); 2) targeting the TRIP13 effector deubiquitinase, USP7; or 3) targeting the USP7 target, NEK2. Our efforts presented here were primarily focused on MM. Given that elevated expression of TRIP13 is observed in many cancers combined with our data in the H1299 lung cancer cell line and the Eμ-*Myc*/*Trip13*^{TG} mouse model, suggest that targeting TRIP13-mediated ubiquitination may have a much broader applications in cancer.

Methods

Establishment of Trip13 transgenic mice

Trip13^{TG} mice were generated at Genome Editing Core Facility of the University of Iowa. We employed the p1026x vector containing the Lck proximal promoter and the immunoglobulin heavy chain intronic enhancer (Eμ). The mouse *Trip13* complete sequenced coding region was inserted into the p1026x vector (a gift from Brian M. Iritani, University of Washington). Briefly, a 10.4 Kb Lck-(Eμ)-m*Trip13*-hGH fragment was inserted into the p1026x vector by Spe1. The modified vector contains a 3.2 kb fragment of the mouse Lck proximal promoter to +37 with respect to the transcription start site (TSS), a 0.92 kb fragment of the Eμ inserted into the Lck fragment, a 2.1 kb mutated (non-translatable) version of the human growth hormone gene (hGH), and the *Trip13* cDNA inserted into the BamH1 site of the Lck promoter fragment. The Lck-(Eμ)-m*Trip13*-hGH fragment is cut out from p1026x vector by Spe1 and injected into C57BL/6 CBA hybrid embryos. Founders were selected by genotyping by PCR from ear tissue DNA with the following Trip13 primers: Forward primer 5' ACC ATG TAC CCA TAC GAT GTT CCA G 3' and reverse primer 5' GCC CTT GTC ATC GTC ATC CTT GTA G 3'. Internal control was employed with the following primers: Forward primer 5' CTA GGC CAC AGA ATT GAA AGA TCT 3' and reverse primer 5' GTA GGT GGA AAT TCT AGC ATCATC C 3'. Three lines were selected and backcrossed to a C57BL/6 background for at least ten generations.

Cell culture

Human myeloma cell lines (ARP1, H929, OCI-MY5 and their derivative cell lines), originally a gift from Dr. John D. Shaughnessy Jr., University of Arkansas for Medical Sciences (Little Rock, Arkansas, USA), were cultured in RPMI 1640 medium (Gibco) supplemented with 10% heat-inactivated FBS (Gibco), penicillin (100 IU/mL) and streptomycin (100μg/mL) in a humidified incubator at 37℃ and 5%CO_2/95% air. HEK293T, H1299 and 3T3 cell lines, a gift from Dr. John D. Shaughnessy Jr., University of Arkansas for Medical Sciences (Little Rock, Arkansas, USA), were cultured with DMEM medium (Gibco) with the same supplements. Primary MM cells were obtained from MM patient BM aspirates by density gradient centrifugation using Ficoll-Paque and purification with CD138 immunomagnetic beads selection with the autoMACs automated separation system (Miltenyi Biotech). Purity of the plasma cells was determined by flow cytometry and aliquots were cryopreserved in liquid nitrogen routinely. Purified MM cells were thawed and cultured in the same condition with myeloma cell lines previously mentioned.

Vectors and transfections

Human *TRIP13* was cloned into the pCDH vector under the promoter of CAG and tagged with 3 x FLAG and HA. The shRNA sequence for TRIP13 were 5'CGATTATGTGATGACAACTTTCTCGAGAAAGTTGTCATCACATAATCGT3' and 5'GCTAATACACTACTGTTGAAAGAGCTCTTTCAACAGTAGTGTATTAGC3' and were inserted into Age1 and EcoR1 sites of doxycycline-inducible expression pLKO-Tet-On shRNA. NEK2 was cloned into the pCMV-AIG vector. TRIP13 deletion constructs (Δ 1: 100 AA deletion form C-terminal and Δ 2: 200 AA deletion form C-terminal) were generated by PCR amplification and cloned using XbaI and BamHI enzymes. USP7-

Flag vector was obtained from Addgene (plasmid #16655). Lentiviruses were packaged in HEK293T cells using VSV-G and psPAX2 helper vectors (Addgene) using calcium phosphate transfection (Promega). Transient transfections were done with Lipofectamine 2000 Reagent (Invitrogen) according to the manufactures guidelines.

Cell lysis, immunoprecipitation and Co-immunoprecipitation

Cell pellets were resuspended in lysis buffer (150 mM NaCl, 10 mM EDTA, 10 mM Tris pH 7.4 and 1% triton X-100 supplemented, Protease inhibitor cocktail, DTT and with 25mM N-Ethylmaleimide) and vortexed vigorously for 10 seconds and incubated on ice for 10 minutes, vortexed again and centrifuged at 13,000 rpm for 10 minutes at 4°C. The cell pellet was discarded and supernatant was analyzed for western blot or frozen at -80°C. For cell fractionations, Nuclear/Cytosol Fractionation kit (BioVision, Inc) was used accordingly to the manufacturer instructions. For immunoprecipitations lysates were collected and the same amounts of protein were incubated either with 25µL of protein A or G dynabeads (Invitrogen) and 3µL of primary antibody overnight. Samples were washed 3 times with IP buffer and eluded by rotating 20 minutes at room temperature with 350mM DTT supplemented sample buffer. Co-Immunoprecipitations were performed using IP buffer (Thermo Scientific) supplemented with the protease inhibitor cocktail. Samples were vortexed for 5 seconds, incubated on ice for 20 minutes, vortexed again and centrifuged 13,000g for 10 minutes at 4°C and supernatants were collected.

Western blot

Protein concentration was calculated by Nanodrop (Thermo Fisher Scientific). Proteins were separated with NuPAGE 4-12% Bis-Tris Gel (NOVEX) at 180V, then transferred to a nitrocellulose membrane for 1 hour at 400 mA at 4°C. Membrane was blocked for 30 minutes with 10% milk at room temperature. Antibodies for anti-USP7 (D17C6 XP, Cell Signaling Technologies,), anti-TRIP13 (C-4: sc-514314, Santa Cruz Biotechnology), anti-NEK2 (D-8: sc-55601, Santa Cruz Biotechnology), anti-ubiquitin (3933S, Cell Signaling Technologies), anti-HA (C29F4, Cell Signaling Technologies), anti-PTEN (D.4.3 XP, Cell Signaling Technologies) and anti-p53 (1C12, Cell Signaling Technologies), anti-GAPDH (14C10, Cell Signaling Technologies), anti-β-ACTIN (D6A8, Cell Signaling Technologies) and anti-H2B (D2H6, Cell Signaling Technologies) were incubated overnight at 4°C with a dilution of 1:500 or 1:1000. Secondary rabbit antibody (Goat anti-rabbit IgG (H+L), HRP-conjugated, Cell Signaling Technologies) and secondary mouse antibody (Goat anti-mouse IgG-HRP: sc-2005, Santa Cruz Biotechnology) were incubated for 1 hour at a concentration of 1: 10,000 at room temperature. For exposure, Immobilon Western HRP Substrate Peroxide Solution from Millipore was used. Imaging was done with ChemiDoc™ XRS+ System with Image Lab Software (BioRad, USA).

In vitro and ex vivo drug treatment conditions

For shRNA induction DOX was used at 100ng/mL for 48 or 72 hours. Bortezomib (Selleckchem), P5091 (Sigama), etoposide (Sigama), melphalan (Sigama), PYR-41 (Selleckchem), PR-619 (Selleckchem) and Spautin-1 (Selleckchem) were used at indicated concentrations for different time period. NEM was solubilized in ethanol and added to lysis buffer immediately before use at a concentration of 10 mM.

Cell viability

For trypan blue staining, 10µL of cell culture was mixed with 10µL of trypan blue. Samples were counted in a hemocytometer, translucent cells were counted as alive and viable, blue stained cells are counted as dead. Cell viability was calculated by dividing viable cells by total cell number, each sample was done in triplicate. For 3-(4, 5-Dimethylthiazol-2-yl)-2, 5-diphenyltetrazolium bromide (MTT) assay, briefly, cells were seeded in 96-well plates and assay performed on triplicated wells for every condition. MTT was then added for 2 hours at a final concentration of 2.5 mg/mL. Plates were centrifuged and the soluble fraction decanted. Crystal pellets were suspended in DMSO and absorbance read at 590 nm and cell viability were presented as percentage normalized to untreated cells.

In vitro de-Ubiquitination

Recombinant USP7 His6 tag (DUB), USP10 His6 tag (DUB), K48- and 63-specific Ubiquitins (pUB) were purchased by Boston Biochem. TRIP13 was not commercial available therefore was isolated from ARP1 TRIP13 OE cells by immunoprecipitation using HA antibodies. For the in vitro deubiquitination four reactions were prepared: **1**. DeUb-buffer (18µL) + pUb (1µg) +deUb buffer (2µL); **2**. DeUb-buffer (18 µL) + pUb (1µg) +DUB (0.1µg) + deUb buffer (1µL), **3**. DeUb-buffer (18µL) + pUb (1µg) + TRIP13 (1µg) + deUb buffer (1µL) and **4**. DeUb-buffer (18µL) + pUb (1µg) +DUB (0.1µg) + TRIP13 (1µg). All these reactions repeated in presence of NEM 25mM. Reaction were mixed by gentle pipetting and incubate at 35°C. After 60 minutes samples were analyzed by western blot. Ponceau S stain was used to determine the efficiency of

transfer. DeUb assay buffer was made from: 50mM Tris-HCl pH7.4, 50mM NaCl, 2mM MgCl2, 1mM DTT and 5% Glycerol.

Mice xenograft models and experiments

For figure 7C, 7D and 7E, 8-10 weeks old NSG mice (Bought from Jackson Laboratories, bred and housed in University of Iowa Animal facility) were subcutaneously injected with 0.5×10^6 ARP1 EV and TRIP13 OE cells into the left and right flank, respectively. Mice were treated with vehicle control, BTZ (1mg/kg, *i.p*., twice a week from day 7), P5091 (10mg/kg, *i.v*., twice a week from day 3) and combination. Mice were sacrificed and tumors were dissected and assessed by week 3.

For figure 8A, 8B and 8C, 8-10 weeks old C57BL/6 mice (Brought from Jackson Laboratories, bred and housed in University of Iowa Animal facility) were injected intravenously with respectively 2×10^6 Eμ-*Myc*/*Trip13*^{WT} and Eμ-*Myc*/*Trip13*^{TG} lymphoma cells via the tail vein on day 0 and treated with Usp7 inhibitor P5091 from 3 days after lymphoma cells injection, doxorubicin once on day 7 and combination of P5091 and doxorubicin, comparing to vehicle control group. P5091 (10 mg/kg, Selleckchem) was injected *i.v.* twice a week. Doxorubicin (10mg/kg, Selleckchem) was injected *i.p*. once on day 7. For survival analyses, treatment of mice continued until an ethical endpoint was reached. Mice were sacrificed at the ethical endpoint: enlarged lymph nodes (approximately palpable diameter of 1cm), loss of weight (more than 20%), labored breathing, hunched posture, ruffled fur, limited mobility or paralysis. For the P5091 and combination groups, P5091 treatment ended when the first mouse in the group reached to the ethical endpoint.

For figure 8D and 8E, to investigate tumor burden after P5091 treatment, 8-10 weeks old CD45.1$^+$ C57BL/6 mice were injected intravenously with 2×10^6 CD45.2$^+$ Eμ-*Myc*/*Trip13*^{TG} lymphoma cells via the tail vein and P5091 treatment was administrated as mentioned above. All mice were sacrificed once the first vehicle control mice got to the ethical endpoint.

Flow cytometry

Mice lymph nodes and spleens were dissected and crushed into single cell suspension in FACS buffer (1x PBS with 2% fetal bovine serum) and filtered through 70 μM cell strainers. Single cell suspension was collected by rinsing with FACS buffer. Cells from spleens were lysed with red blood cell lysis buffer (KD medical) to remove red blood cells. After washing with 1x PBS, 0.5-1×10^6 cells were resuspended in 100 μL FACS buffer and pre-incubated with anti-mouse CD16/32 antibody (Biolegend) for blocking prior to labeling with antibodies of CD45.2-PerCP-Cy5.5, CD45.1-PE, B220-APC-Cy7 and IgM-FITC (Biolegend) for 20 min at 4°C. Cells were then washed with FACS buffer and analyzed on BD LSR II UV at The University of Iowa flow cytometry facility. All flow results were analyzed using FlowJo software (Version 9).

Microarray data sets

Gene expression profiling data were obtained from previous studies and are available under the NCBI's Gene Expression Omnibus under accession numbers GSE2658 (1) and GSE10846 (51).

Statistics

Mouse survival analysis and patient survival analysis were carried out using GraphPad Prism software (Version 8.0), and significance determined using log-rank (Mantel-Cox) test. All other statistical comparisons were analyzed by unpaired, 2-tailed, independent Student's *t* test, unless otherwise described in the figure legends. A *P* value less than 0.05 was considered significant. Results are presented as mean ± SD and *n* is indicated in figure legends.

Study approval

NSG mice (Jackson Laboratories) were bred and maintained in compliance with the guidelines of the institutional animal care at the University of Iowa. The animal studies were performed according to the guidelines of the Institutional Animal Care and local veterinary office and ethics committee of the University of Iowa, USA under approved protocol (IACUC 5081482). De-identified primary samples were obtained from MM patients during UAMS clinic visits. Signed institutional review board-approved informed consent forms are kept on record in UAMS Tissue Biorepository and Procurement Service (TBAPS) under approved protocol IRB #260731.

Author contributions

C.L. performed the experiments, collected, analyzed the data, generated the figures, wrote and edited the manuscript; J.X. and R.F.M. performed experiments and analyzed the data; F.C. and Y.H. reviewed the data and edited the manuscript; T.C.A. and F.T. analyzed the RNA-sequencing data. H.X. maintained the mouse strains and analyzed the data; D.L., D.G., S.K.J and F.vR. reviewed the data; J.D.S. and G.T. reviewed the data and edited the manuscript; I.F. performed experiments, designed and supervised experiments and analyzed data; F.Z. designed and supervised this study, collected and analyzed data, wrote and edited the manuscript.

Acknowledgments

This work was supported by NCI R01CA236814 (to F.Z.), US DoD CA180190 (to F.Z.), Leukemia and Lymphoma Society TRP 6549-18 (to F.Z.), Myeloma Crowd Research Initiative Award (to F.Z.), Riney Family Multiple Myeloma Research Program Fund (to F.Z.), NCI R01CA151354 (to S.J.) and UAMS Winthrop P. Rockefeller Cancer Institute start-up (to F. Z.). We would like to thank Dr. Hasem Habelhah, University of Iowa, for providing us the protocol of in vitro ubiquitination assay, Dr. Zhimin Gu for making the Lck-(Eμ)-m*Trip13*-hGH/p1026x construct to generate transgenic mice and the support of UAMS Tissue Biorepository and Procurement Core and UAMS Proteomics Core.

References

1. Shaughnessy JD, Jr., Zhan F, Burington BE, Huang Y, Colla S, Hanamura I, et al. A validated gene expression model of high-risk multiple myeloma is defined by deregulated expression of genes mapping to chromosome 1. *Blood.* 2007;109(6):2276-84.

2. Kumar SK, Dimopoulos MA, Kastritis E, Terpos E, Nahi H, Goldschmidt H, et al. Natural history of relapsed myeloma, refractory to immunomodulatory drugs and proteasome inhibitors: a multicenter IMWG study. *Leukemia.* 2017;31(11):2443-8.

3. Rajkumar SV. Multiple myeloma: 2012 update on diagnosis, risk-stratification, and management. *Am J Hematol.* 2012;87(1):78-88.

4. Barlogie B, Mitchell A, van Rhee F, Epstein J, Morgan GJ, and Crowley J. Curing myeloma at last: defining criteria and providing the evidence. *Blood.* 2014;124(20):3043-51.

5. Hanamura I, Stewart JP, Huang Y, Zhan F, Santra M, Sawyer JR, et al. Frequent gain of chromosome band 1q21 in plasma-cell dyscrasias detected by fluorescence in situ hybridization: incidence increases from MGUS to relapsed myeloma and is related to prognosis and disease progression following tandem stem-cell transplantation. *Blood.* 2006;108(5):1724-32.

6. Zhou W, Yang Y, Xia J, Wang H, Salama ME, Xiong W, et al. NEK2 induces drug resistance mainly through activation of efflux drug pumps and is associated with poor prognosis in myeloma and other cancers. *Cancer Cell.* 2013;23(1):48-62.

7. Tao Y, Yang G, Yang H, Song D, Hu L, Xie B, et al. TRIP13 impairs mitotic checkpoint surveillance and is associated with poor prognosis in multiple myeloma. *Oncotarget.* 2017;8(16):26718-31.

8. Heuck CJ, Qu P, van Rhee F, Waheed S, Usmani SZ, Epstein J, et al. Five gene probes carry most of the discriminatory power of the 70-gene risk model in multiple myeloma. *Leukemia.* 2014;28(12):2410-3.

9. Zhou K, Zhang W, Zhang Q, Gui R, Zhao H, Chai X, et al. Loss of thyroid hormone receptor interactor 13 inhibits cell proliferation and survival in human chronic lymphocytic leukemia. *Oncotarget.* 2017;8(15):25469-81.

10. Larkin SE, Holmes S, Cree IA, Walker T, Basketter V, Bickers B, et al. Identification of markers of prostate cancer progression using candidate gene expression. *Br J Cancer.* 2012;106(1):157-65.

11. Dong L, Ding H, Li Y, Xue D, Li Z, Liu Y, et al. TRIP13 is a predictor for poor prognosis and regulates cell proliferation, migration and invasion in prostate cancer. *Int J Biol Macromol.* 2019;121:200-6.

12. Rhodes DR, Yu J, Shanker K, Deshpande N, Varambally R, Ghosh D, et al. Large-scale meta-analysis of cancer microarray data identifies common transcriptional profiles of neoplastic transformation and progression. *Proc Natl Acad Sci U S A.* 2004;101(25):9309-14.

13. Martin KJ, Patrick DR, Bissell MJ, and Fournier MV. Prognostic breast cancer signature identified from 3D culture model accurately predicts clinical outcome across independent datasets. *PLoS One.* 2008;3(8):e2994.

14. Abdul Aziz NA, Mokhtar NM, Harun R, Mollah MM, Mohamed Rose I, Sagap I, et al. A 19-Gene expression signature as a predictor of survival in colorectal cancer. *BMC Med Genomics.* 2016;9(1):58.

15. Yao J, Zhang X, Li J, Zhao D, Gao B, Zhou H, et al. Silencing TRIP13 inhibits cell growth and metastasis of hepatocellular carcinoma by activating of TGF-beta1/smad3. *Cancer Cell Int.* 2018;18:208.

16. Kang JU, Koo SH, Kwon KC, Park JW, and Kim JM. Gain at chromosomal region 5p15.33, containing TERT, is the most frequent genetic event in early stages of non-small cell lung cancer. *Cancer Genet Cytogenet.* 2008;182(1):1-11.

17. Zhang Q, Dong Y, Hao S, Tong Y, Luo Q, and Aerxiding P. The oncogenic role of TRIP13 in regulating proliferation, invasion, and cell cycle checkpoint in NSCLC cells. *Int J Clin Exp Pathol.* 2019;12(9):3357-66.

18. Banerjee R, Russo N, Liu M, Basrur V, Bellile E, Palanisamy N, et al. TRIP13 promotes error-prone nonhomologous end joining and induces chemoresistance in head and neck cancer. *Nat Commun.* 2014;5:4527.

19. Vader G. Pch2(TRIP13): controlling cell division through regulation of HORMA domains. *Chromosoma.* 2015;124(3):333-9.

20. Clairmont CS, Sarangi P, Ponnienselvan K, Galli LD, Csete I, Moreau L, et al. TRIP13 regulates DNA repair pathway choice through REV7 conformational change. *Nat Cell Biol.* 2020;22(1):87-96.

21. Shaughnessy JD, Jr., Qu P, Usmani S, Heuck CJ, Zhang Q, Zhou Y, et al. Pharmacogenomics of bortezomib test-dosing identifies hyperexpression of proteasome genes, especially PSMD4, as novel high-risk feature in myeloma treated with Total Therapy 3. *Blood.* 2011;118(13):3512-24.

22. Barbagallo F, Paronetto MP, Franco R, Chieffi P, Dolci S, Fry AM, et al. Increased expression and nuclear localization of the centrosomal kinase Nek2 in human testicular seminomas. *J Pathol.* 2009;217(3):431-41.

23. Stricker TP, Henriksen KJ, Tonsgard JH, Montag AG, Krausz TN, and Pytel P. Expression profiling of 519 kinase genes in matched malignant peripheral nerve sheath tumor/plexiform neurofibroma samples is discriminatory and identifies mitotic regulators BUB1B, PBK and NEK2 as overexpressed with transformation. *Mod Pathol.* 2013;26(7):930-43.

24. Meng L, Carpenter K, Mollard A, Vankayalapati H, Warner SL, Sharma S, et al. Inhibition of Nek2 by small molecules affects proteasome activity. *Biomed Res Int.* 2014;2014:273180.

25. Franqui-Machin R, Hao M, Bai H, Gu Z, Zhan X, Habelhah H, et al. Destabilizing NEK2 overcomes resistance to proteasome inhibition in multiple myeloma. *J Clin Invest.* 2018;128(7):2877-93.

26. Hao M, Franqui-Machin R, Xu H, Shaughnessy J, Jr., Barlogie B, Roodman D, et al. NEK2 induces osteoclast differentiation and bone destruction via heparanase in multiple myeloma. *Leukemia.* 2017;31(7):1648-50.

27. Iritani BM, Forbush KA, Farrar MA, and Perlmutter RM. Control of B cell development by Ras-mediated activation of Raf. *Embo j.* 1997;16(23):7019-31.

28. Dang CV. MYC on the path to cancer. *Cell.* 2012;149(1):22-35.

29. Misund K, Keane N, Stein CK, Asmann YW, Day G, Welsh S, et al. MYC dysregulation in the progression of multiple myeloma. *Leukemia.* 2020;34(1):322-6.

30. Horn H, Ziepert M, Becher C, Barth TF, Bernd HW, Feller AC, et al. MYC status in concert with BCL2 and BCL6 expression predicts outcome in diffuse large B-cell lymphoma. *Blood.* 2013;121(12):2253-63.

31. Harris AW, Pinkert CA, Crawford M, Langdon WY, Brinster RL, and Adams JM. The E mu-myc transgenic mouse. A model for high-incidence spontaneous lymphoma and leukemia of early B cells. *J Exp Med.* 1988;167(2):353-71.

32. Rempel RE, Jiang X, Fullerton P, Tan TZ, Ye J, Lau JA, et al. Utilization of the Emu-Myc mouse to model heterogeneity of therapeutic response. *Mol Cancer Ther.* 2014;13(12):3219-29.

33. Alizadeh AA, Eisen MB, Davis RE, Ma C, Lossos IS, Rosenwald A, et al. Distinct types of diffuse large B-cell lymphoma identified by gene expression profiling. *Nature.* 2000;403(6769):503-11.

34. Schmitz R, Wright GW, Huang DW, Johnson CA, Phelan JD, Wang JQ, et al. Genetics and Pathogenesis of Diffuse Large B-Cell Lymphoma. *N Engl J Med.* 2018;378(15):1396-407.

35. Zhou J, Wang J, Chen C, Yuan H, Wen X, and Sun H. USP7: Target Validation and Drug Discovery for Cancer Therapy. *Med Chem.* 2018;14(1):3-18.

36. Song MS, Salmena L, Carracedo A, Egia A, Lo-Coco F, Teruya-Feldstein J, et al. The deubiquitinylation and localization of PTEN are regulated by a HAUSP-PML network. *Nature.* 2008;455(7214):813-7.

37. Li M, Chen D, Shiloh A, Luo J, Nikolaev AY, Qin J, et al. Deubiquitination of p53 by HAUSP is an important pathway for p53 stabilization. *Nature.* 2002;416(6881):648-53.

38. Alfieri C, Chang L, and Barford D. Mechanism for remodelling of the cell cycle checkpoint protein MAD2 by the ATPase TRIP13. *Nature.* 2018;559(7713):274-8.

39. Symersky J, Osowski D, Walters DE, and Mueller DM. Oligomycin frames a common drug-binding site in the ATP synthase. *Proc Natl Acad Sci U S A.* 2012;109(35):13961-5.

40. Ye Q, Rosenberg SC, Moeller A, Speir JA, Su TY, and Corbett KD. TRIP13 is a protein-remodeling AAA+ ATPase that catalyzes MAD2 conformation switching. *Elife.* 2015;4.

41. Popovic D, Vucic D, and Dikic I. Ubiquitination in disease pathogenesis and treatment. *Nat Med.* 2014;20(11):1242-53.

42. Mallette FA, and Richard S. K48-linked ubiquitination and protein degradation regulate 53BP1 recruitment at DNA damage sites. *Cell Res.* 2012;22(8):1221-3.

43. Ohtake F, Tsuchiya H, Saeki Y, and Tanaka K. K63 ubiquitylation triggers proteasomal degradation by seeding branched ubiquitin chains. *Proc Natl Acad Sci U S A.* 2018;115(7):E1401-E8.

44. Ernst R, Mueller B, Ploegh HL, and Schlieker C. The otubain YOD1 is a deubiquitinating enzyme that associates with p97 to facilitate protein dislocation from the ER. *Mol Cell.* 2009;36(1):28-38.

45. Wang Y, Satoh A, Warren G, and Meyer HH. VCIP135 acts as a deubiquitinating enzyme during p97-p47-mediated reassembly of mitotic Golgi fragments. *J Cell Biol.* 2004;164(7):973-8.

46. Trotman LC, Wang X, Alimonti A, Chen Z, Teruya-Feldstein J, Yang H, et al. Ubiquitination regulates PTEN nuclear import and tumor suppression. *Cell.* 2007;128(1):141-56.

47. Cummins JM, and Vogelstein B. HAUSP is required for p53 destabilization. *Cell Cycle.* 2004;3(6):689-92.

48. Li M, Brooks CL, Kon N, and Gu W. A dynamic role of HAUSP in the p53-Mdm2 pathway. *Mol Cell.* 2004;13(6):879-86.

49. Shen Y, Tu W, Liu Y, Yang X, Dong Q, Yang B, et al. TSPY1 suppresses USP7-mediated p53 function and promotes spermatogonial proliferation. *Cell Death Dis.* 2018;9(5):542.

50. Wang Y, Huang J, Li B, Xue H, Tricot G, Hu L, et al. A Small-Molecule Inhibitor Targeting TRIP13 Suppresses Multiple Myeloma Progression. *Cancer Res.* 2020;80(3):536-48.

51. Lenz G, Wright G, Dave SS, Xiao W, Powell J, Zhao H, et al. Stromal gene signatures in large-B-cell lymphomas. *N Engl J Med.* 2008;359(22):2313-23.

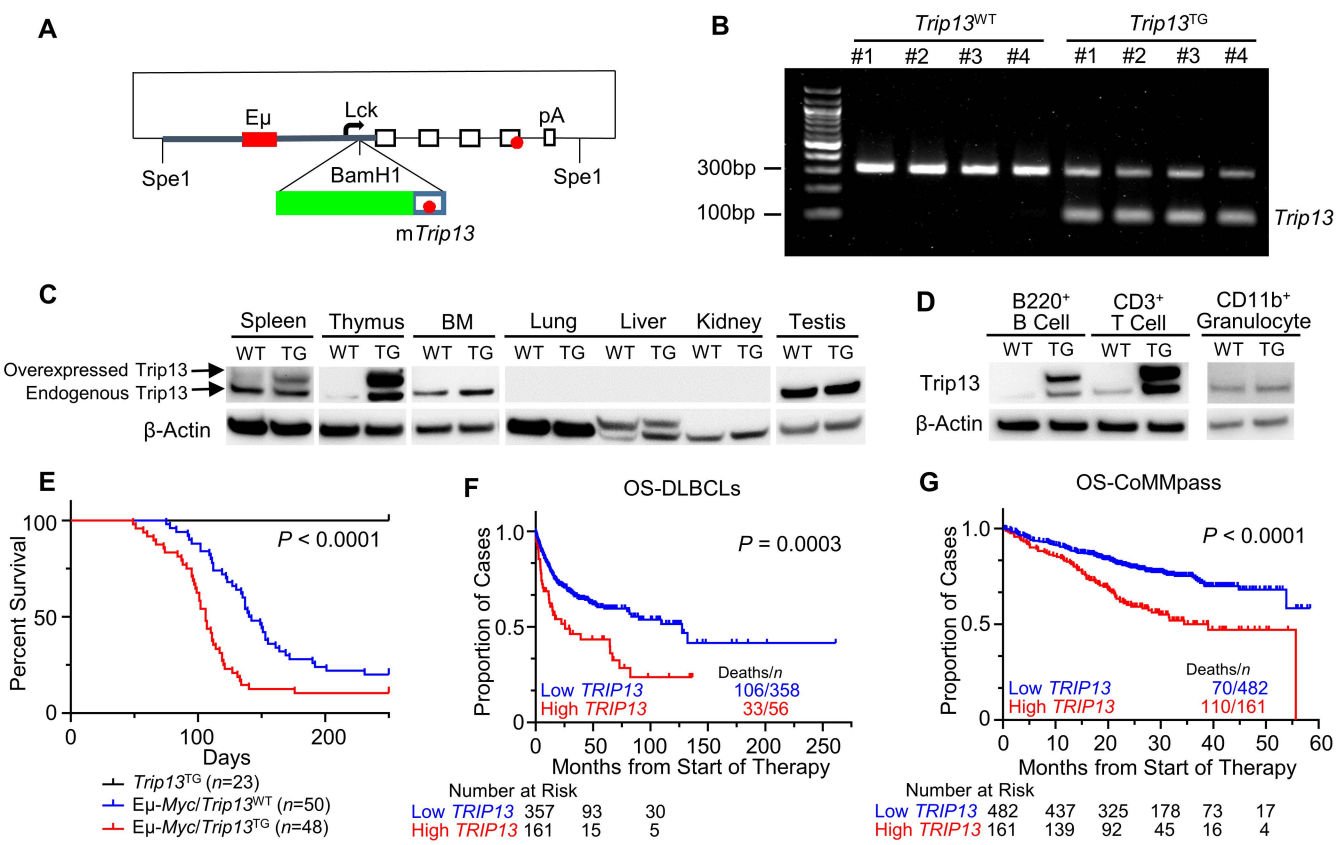

Figure 1. TRIP13 accelerates tumorigenesis in Eμ-*Myc* mouse model and is linked to poor prognosis in patients with B-cell malignancies. (**A**) Schematic diagram of the modified p1026x vector. Briefly, a 10.4 Kb Lck-(Eμ)-m*Trip13*-hGH fragment was inserted into the p1026x vector by Spe1. The modified vector contains a 3.2 kb fragment of the mouse *Lck* proximal promoter to +37 with respect to the transcription start site (TSS) (thick grey line), a 0.92 kb fragment of the immunoglobulin heavy chain intronic enhancer (Eμ) (solid red box) inserted into the Lck fragment, a 2.1 kb mutated (non-translatable) version of the human growth hormone gene (hGH) (open boxes), and the *Trip13* cDNA (green box) inserted into the BamH1 site of the Lck promoter fragment. The poly-adenylation site of the hGH gene is indicated. Stop codons in the *Trip13* cDNA and hGH genes are indicated by red circles. (**B**) Genotyping of *Trip13* transgenic (*Trip13*^{TG}) mice performed on ear tissue DNA by PCR. The 324 bp band for *Trip13*^{WT} and the 100 bp band for *Trip13*^{TG} are indicated. (**C**) Western blot analysis of Trip13 protein in different tissues of *Trip13*^{TG} and *Trip13*^{WT} mice. (**D**) Western blot analysis of Trip13 protein in B220^{+} B-cells, CD3^{+} T-cells and CD11b^{+} granulocytes of *Trip13*^{TG} and *Trip13*^{WT} mice. (**E**) Kaplan-Meier analysis of *Trip13*^{TG} (*n*=23), Eμ-*Myc/Trip13*^{WT} (*n*=50) and Eμ-*Myc/Trip13*^{TG} (*n*=48) mice ($P < 0.0001$ by log-rank test. The number of evaluated mice is indicated between parentheses). (**F**) Kaplan-Meier analysis of DLBCLs patients with high versus low *TRIP13* (Best cut off, $P = 0.0003$ by log-rank test). (**G**) Kaplan-Meier analysis of MM patients with high (Quartile 4) versus low (Quartile 1-3) *TRIP13* ($P < 0.0001$ by log-rank test).

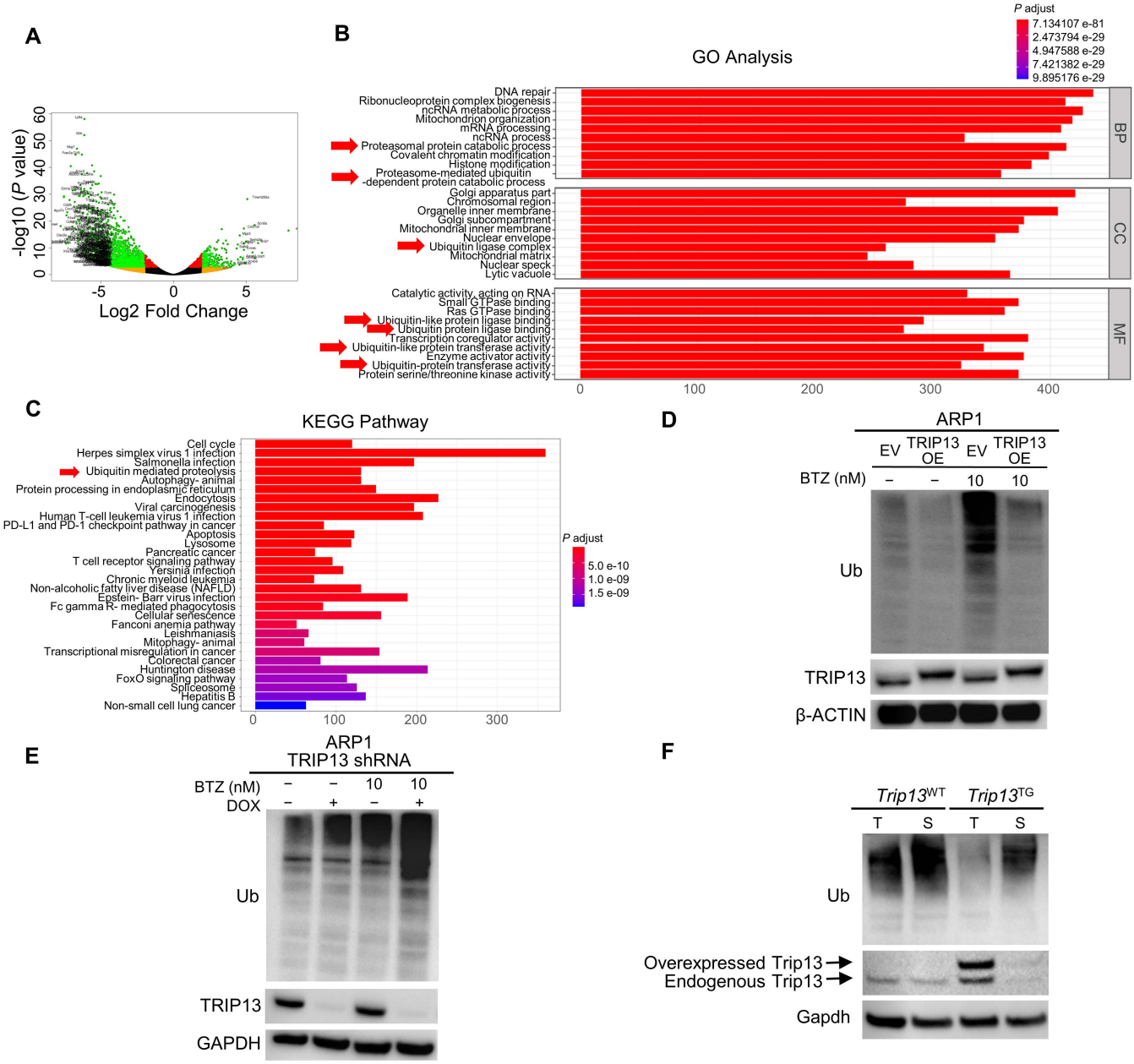

Figure 2. TRIP13 enhances cellular protein deubiquitination. Representational and pathway analysis of approximately 1900 differentially expressed genes in B cells from Eμ-*Myc*/*Trip13*^{TG} versus Eμ-*Myc*/*Trip13*^{WT} mice ($P < 0.001$) displayed in (**A**) Volcano plot and bar graphs of (**B**) GO terms and (**C**) KEGG pathways. Ubiquitin (Ub) and proteasome related terms or pathways are indicated by red arrows. (**D**) Western blot analysis of Ub, TRIP13 and β-ACTIN in EV and TRIP13 OE ARP1 cells treated overnight with or without 10nM BTZ. (**E**) Western blot analysis of Ub, TRIP13 and GAPDH in ARP1 cells transfected with a DOX-inducible TRIP13 shRNA, treated with or without DOX for 72hr, followed by treatment with or without 10nM BTZ. (**F**) Western blot analysis of Ub, Trip13 and Gapdh in thymus (T) and spleen (S) from *Trip13*^{TG} and *Trip13*^{WT} mice.

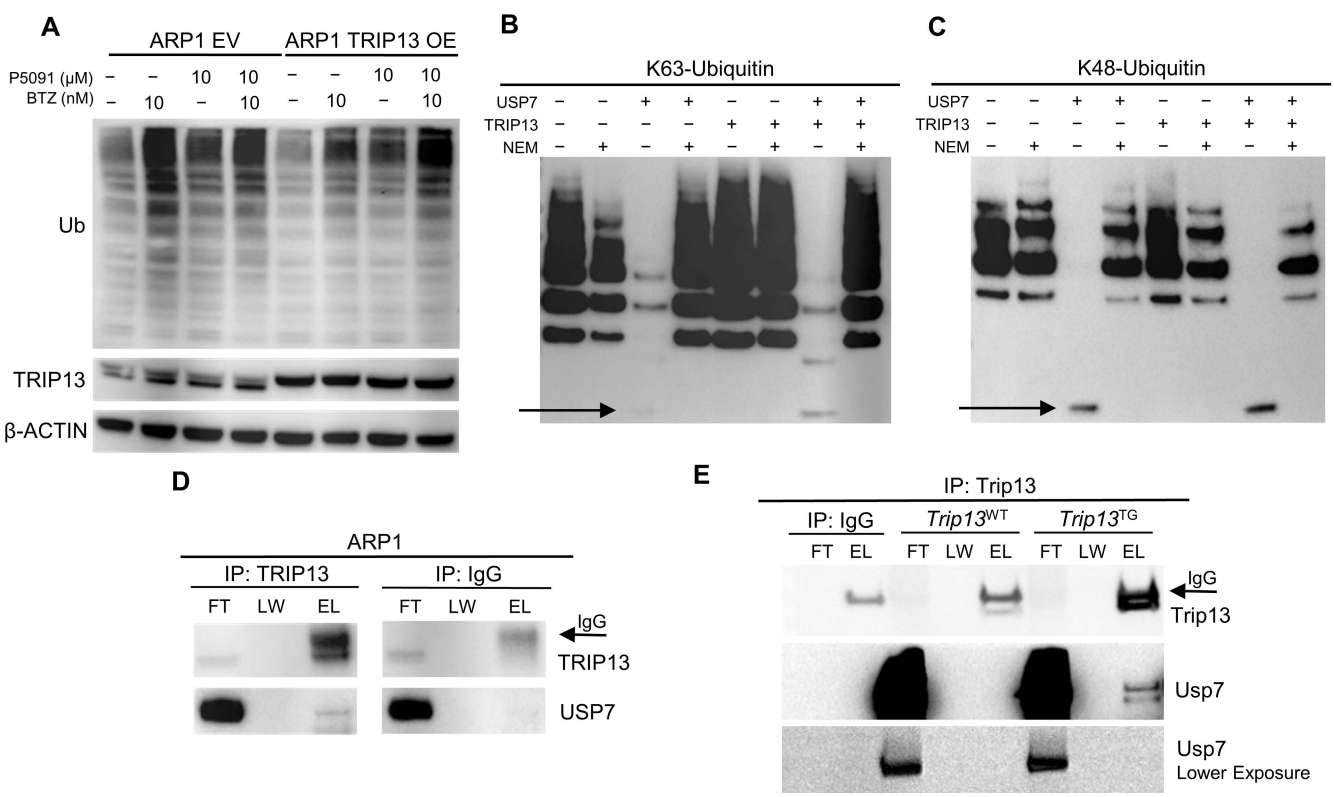

Figure 3. TRIP13 enhances cellular deubiquitination by binding USP7. (**A**) Western blot analysis of Ub, TRIP13 and β-ACTIN in EV and TRIP13 OE ARP1 cells treated overnight with or without 10nM BTZ or 10μM P5091 alone or in combination. (**B**) and (**C**) Western blot analysis of Ubiquitin following USP7 deubiquitination of recombinant K63-Ubiquitin or K48-Ubiquitin in the presence or absence of purified TRIP13 and NEM. (**D**) TRIP13 immunoprecipitation in ARP1 cells. Western blots of flow through (FT), last wash (LW) and elution (E) of the immunoprecipitation were probed with TRIP13 and USP7 antibodies. Arrow indicates non-specific IgG band. (**E**) Trip13 immunoprecipitation from thymus of *Trip13*^{TG} and *Trip13*^{WT} mice. Western blots were probed for Trip13 and Usp7 antibodies.

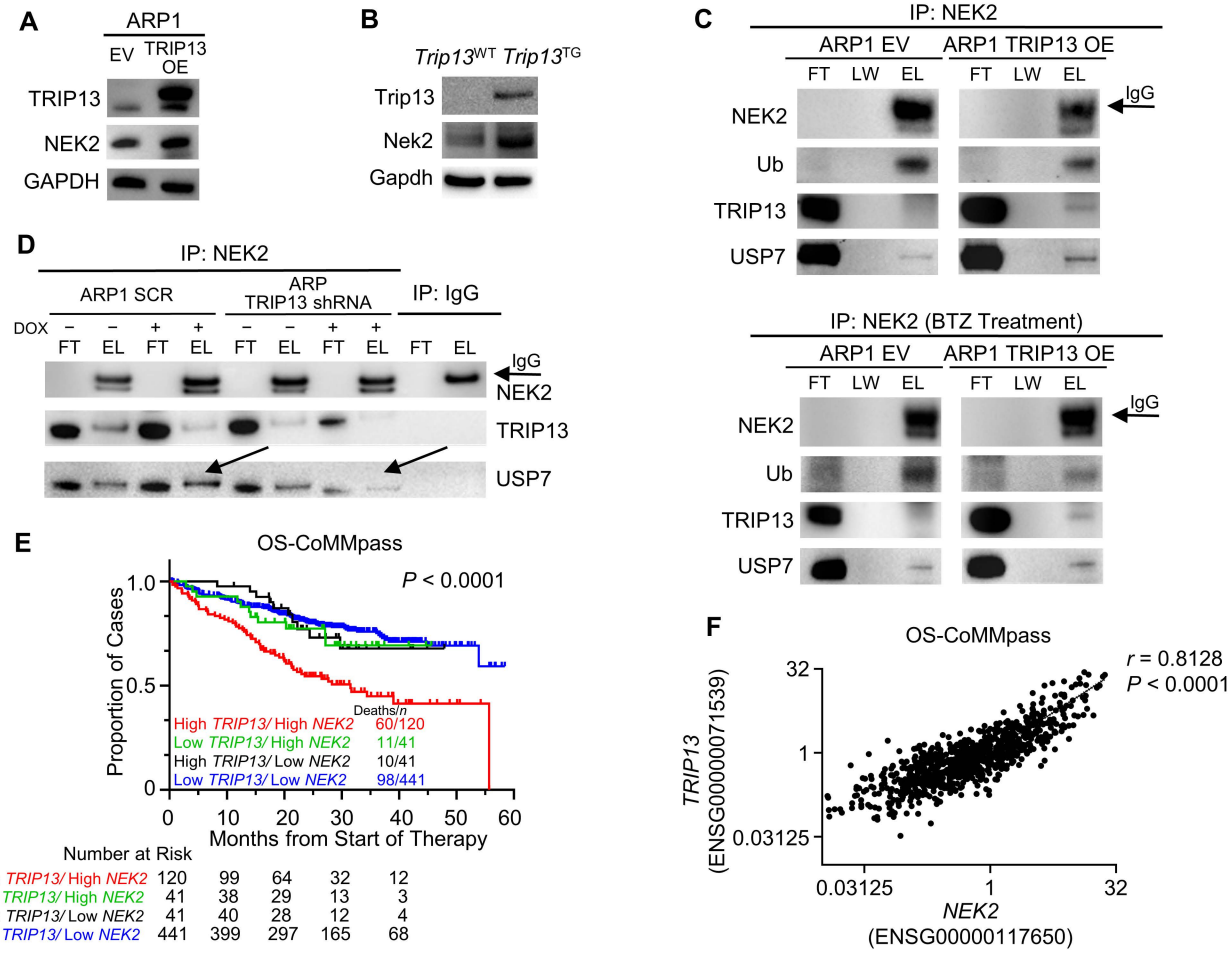

Figure 4. TRIP13 plays a critical role in stabilizing the USP7 target, NEK2. Western blot analysis of TRIP13, NEK2 and GAPDH in (**A**) ARP1 EV and TRIP13 OE cells and (**B**) tissues from *Trip13*^{TG} and *Trip13*^{WT} mice. (**C**) NEK2 immunoprecipitation from ARP1 EV and TRIP13 OE cells treated with or without 10nM BTZ for 1 hour followed by western blot analysis of NEK2, Ub, TRIP13 and USP7. (**D**) NEK2 immunoprecipitation from ARP1 cells stably expressing Scramble (SCR) or TRIP13 shRNA treated with or without DOX for 48 hours followed by western blot analysis of NEK2, TRIP13 and USP7. Arrows indicate the reduction in USP7 signal after TRIP13 shRNA induction. (**E**) Kaplan-Meier analysis of MM patients with high *TRIP13* and high *NEK2* versus MM with one or both genes low ($P < 0.0001$ by log-rank test). (**F**) Scatter plot of *NEK2* and *TRIP13* gene expression intensities from the CoMMpass dataset. Pearson's correlation (r) value and corresponding P value are indicated.

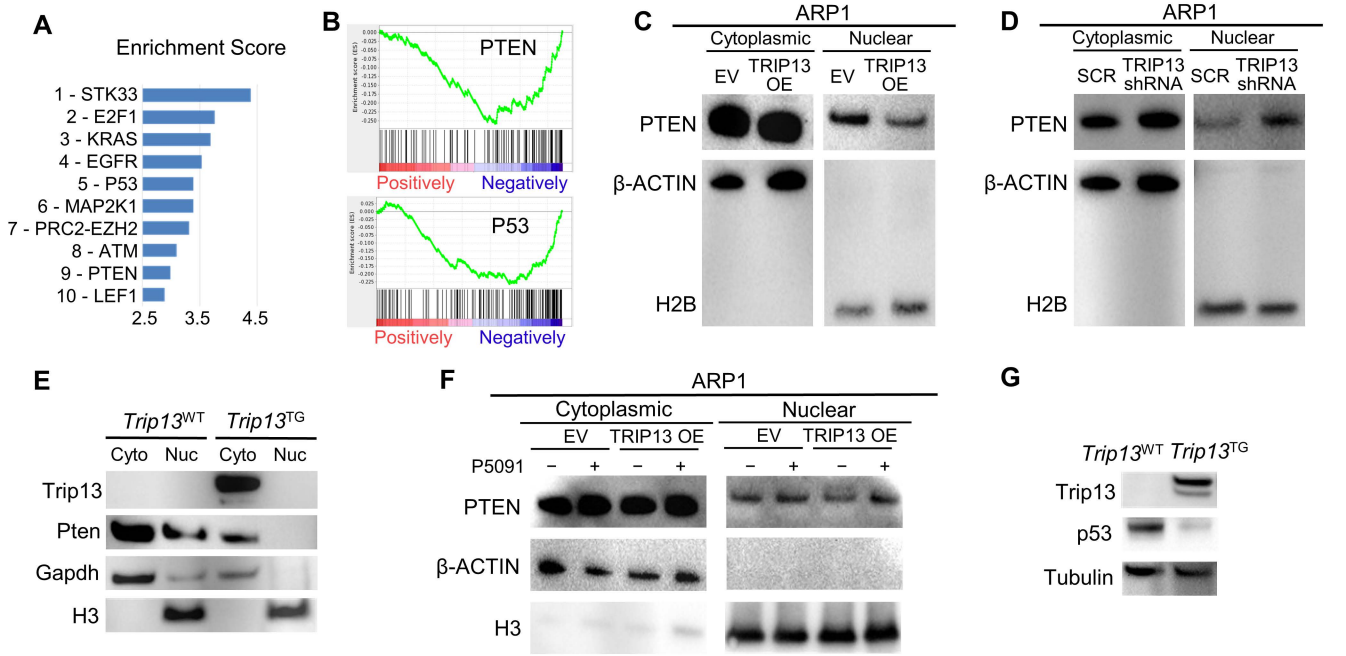

Figure 5. TRIP13 dysregulates other USP7 targets. Gene Set Enrichment Analysis (GSEA) of the 1900 most significantly differentially expressed genes in comparison of Eμ-*Myc*/*Trip13*^{TG} and Eμ-*Myc*/*Trip13*^{WT} B-cells showing (**A**) a bar view the top 10 pathways and (**B**) an enrichment plot for PTEN (upper plot) and p53 pathways (lower plot) indicating suppression of these pathways when *Trip13* is overexpressed. Western blot analysis of PTEN, β-ACTIN and Histone 2B (H2B) from nuclear and cytosolic fractions of (**C**) EV and TRIP13 OE ARP1 cells and (**D**) ARP1 cells stably transduced with SCR and TRIP13 shRNA after 72 hours induction with DOX. (**E**) Western blot analysis of Trip13, Pten, Gapdh and Histone 3 (H3) from nuclear and cytosolic fractions of thymus from *Trip13*^{TG} and *Trip13*^{WT}mice. (**F**) Western blot analysis of PTEN, β-ACTIN and H3 in nuclear and cytosolic fractions from EV and TRIP13 OE ARP1 MM cells treated with 16μM P5091 for 5h. (**G**) Western blot analysis of Trip13, p53 and tubulin in thymus tissues from *Trip13*^{TG} and *Trip13*^{WT} mice.

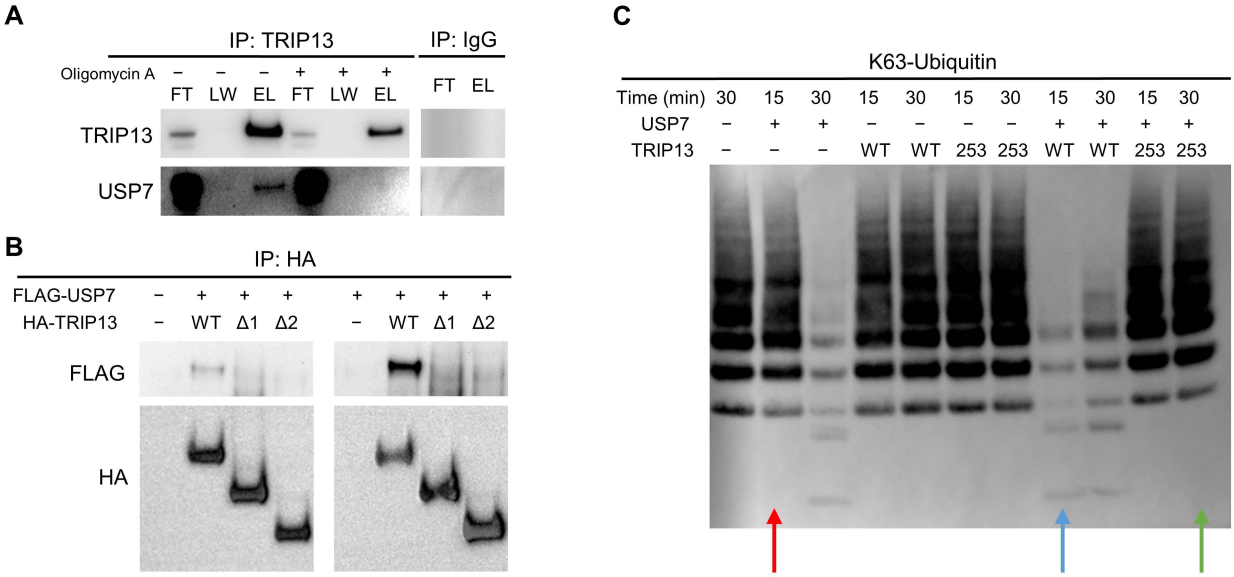

Figure 6. The AAA⁺-ATPase of TRIP13 is required for USP7 deubiquitinase function. (**A**) TRIP13 immunoprecipitation of ARP1 TRIP13 OE cells treated with oligomycin A for 6 hours followed by western blot analysis of FT, LW and E for TRIP13 and USP7. (**B**) TRIP13 immunoprecipitation from HEK293T cells transduced with FLAG-USP7 or FLAG-USP7 and wild-type HA-TRIP13 (WT), truncation 1 (Δ1) HA-TRIP13 or truncation 2 (Δ2) HA-TRIP13 followed by western blot analysis of FLAG or HA. (**C**) Deubiquitination time course and western blot analysis of Ubiquitin derived from recombinant K63-Ubiquitin in the presence of recombinant USP7 with or without purified TRIP13 wild-type (WT) or TRIP13 E253Q mutant (253).

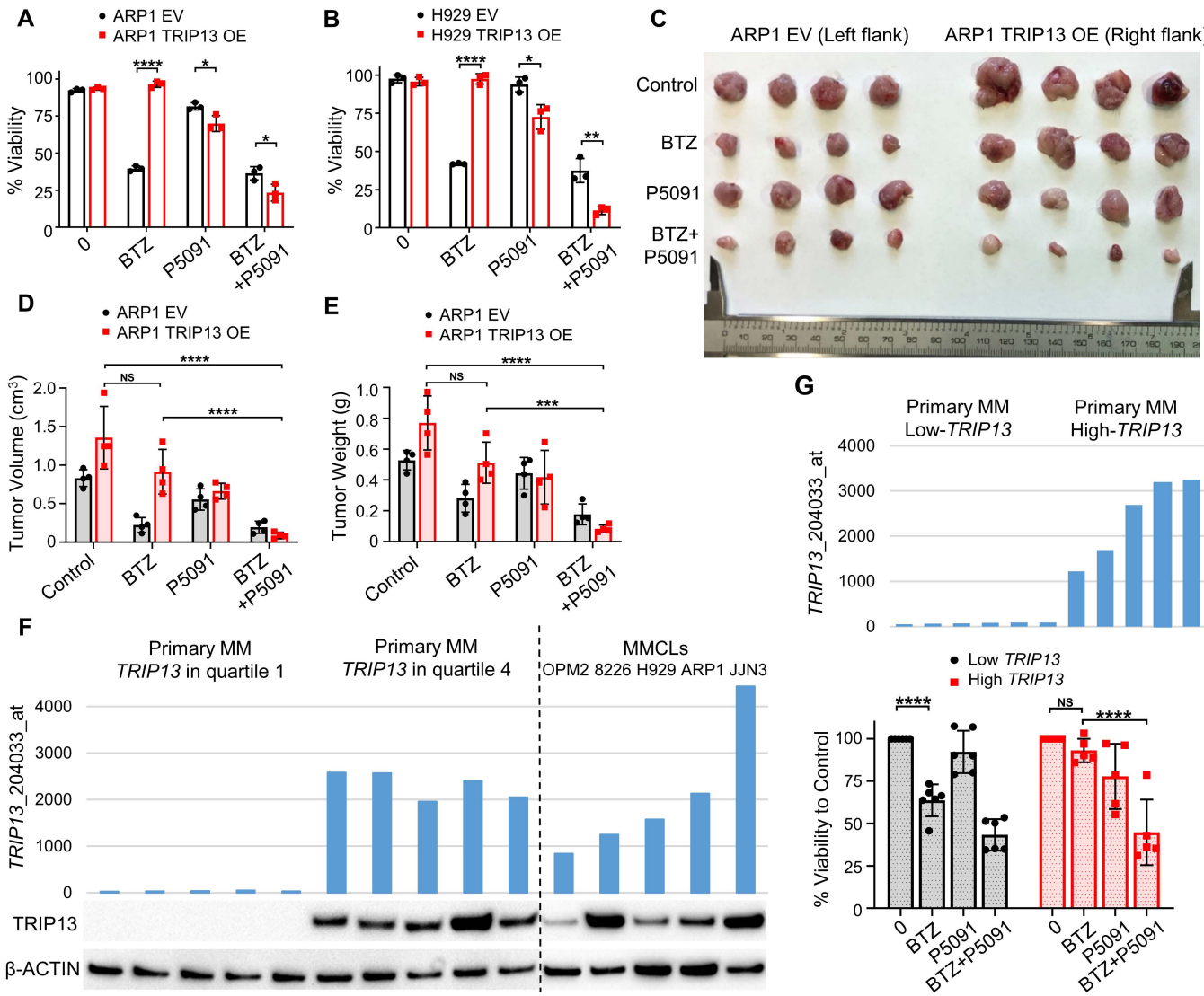

Figure 7. The USP7 inhibitor P5091 reduces TRIP13-induced BTZ drug resistance in MM. ARP1 (**A**) and H929 (**B**) EV and TRIP13 OE cells treated with or without 10nM BTZ or 10μM P5091 alone or in combination for 48h followed by cell viability determination by trypan blue staining (n = 3 per condition). (**C**) ARP1 EV and TRIP13 OE cells (~0.5 × 10^6 cells/injection) were injected into the left and right flanks of NSG mice, respectively. Mice were treated with vehicle control, BTZ (1mg/kg, *i.p.*, twice a week from day 7), P5091 (10mg/kg, *i.v.*, twice a week from day 3) and in combination. Mice were sacrificed and tumors were dissected and photographed by week 3 (n = 4 per group). Tumor volume (**D**) and tumor weight (**E**) were measured and quantified from (**C**). (**F**) *TRIP13* gene expression signal is plotted on the *y*-axis. Primary MM with *TRIP13* expression in quartile 1 (n =5) and quartile 4 (n = 5) and MM cell lines (MMCLs, n = 5) are grouped and plotted along the *x*-axis. Corresponding TRIP13 and β-ACTIN protein level was analyzed from cell lysates of aliquot CD138-positive cells and MMCLs by western blot. (**G**) *TRIP13* gene expression signal of primary MM with low *TRIP13* expression in quartile 1 (n=6) and high *TRIP13* expression in quartile 4 (n=5) is plotted on the *y*-axis. Corresponding CD138-positive cells were treated with or without 5nM BTZ or 2.5μM P5091 alone or in combination for 24h followed by cell viability determination by trypan blue staining. One high *TRIP13* sample was excluded due to low cell viability after thawing. Data are represented as mean ± SD. * $P \le 0.05$, ** $P \le 0.01$, *** $P \le 0.001$, **** $P \le 0.0001$, NS no significance by Student's t test in (**A**), (**B**) and by Tukey's test for multiplicity adjusted P values in (**D**), (**E**) and (**G**).

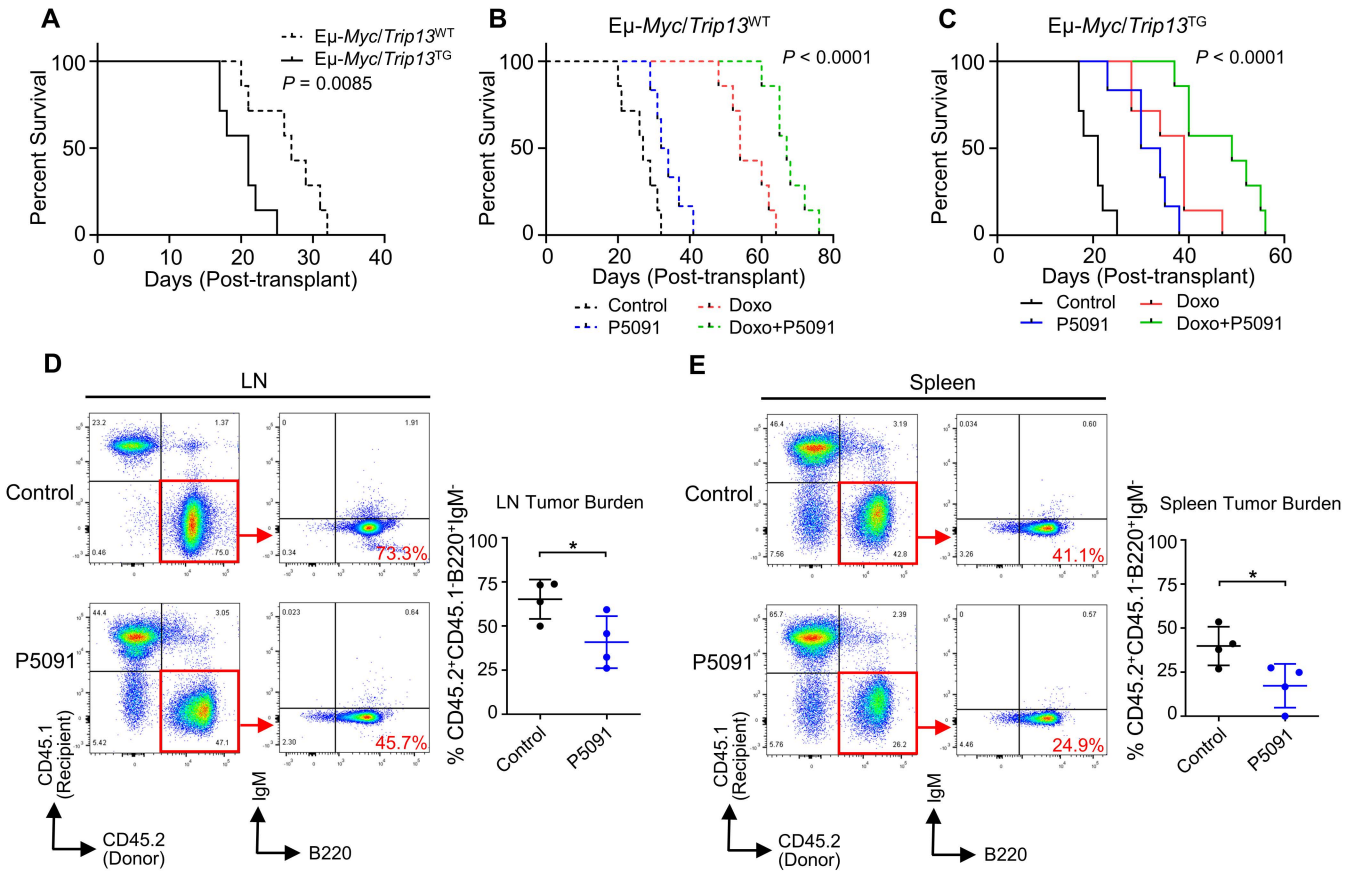

Figure 8. Pharmacological inhibition of Usp7 improves survival and abrogates lymphoma growth in transplanted *Myc*-driven B-cell lymphomas in vivo. Kaplan-Meier analysis of: (**A**) C57BL/6 mice transplanted with Eμ-*Myc* lymphoma cells [Clone #1 (*Trip13*^{WT}, dotted lines) and clone #2 (*Trip*13^{TG}, solid lines)]. Eμ-*Myc*/*Trip13*^{WT} or Eμ-*Myc*/*Trip13*^{TG} lymphoma transplanted mice treated with vehicle control; (**B**) Eμ-*Myc*/*Trip13*^{WT} or (**C**) Eμ-*Myc*/*Trip13*^{TG} lymphoma transplanted mice treated with vehicle control (black lines), P5091 (10mg/kg, *i.v.*, twice a week from day 3 after transplant, blue lines), doxorubicin (Doxo, 10mg/kg, *i.p.*, once on day 7 after transplant, red lines) and in combination (green lines) (*P* values between all groups of each cohort are indicated by log-rank test. *n* = 6-7 per group). Representative flow cytometry plots demonstrating the loss of Eμ-*Myc*/*Trip13*^{TG} donor lymphoma cells (CD45.2^{+}CD45.1^{-} B220^{+}IgM^{-}) after P5091 treatment in CD45.1^{+} recipient mouse lymph node (**D**) and spleen (**E**) tumor tissues (Data are represented as mean ± SD. * *P* < 0.05 by Student's *t* test. *n* = 4 per group).